IOP PUBLISHING PHYSICS IN MEDICINE AND BIOLOGY

Phys. Med. Biol. **54** (2009) 4835–4848 doi:10.1088/0031-9155/54/15/013

Influence of the surface averaging procedure of the current density in assessing compliance with the ICNIRP low-frequency basic restrictions by means of numerical techniques

N Zoppetti and D Andreuccetti

IFAC-CNR ('Nello Carrara' Institute for Applied Physics of the Italian National Research Council), Via Madonna del Piano 10, 50019 Sesto Fiorentino (FI), Italy

E-mail: N.Zoppetti@ifac.cnr.it and D.Andreuccetti@ifac.cnr.it

Received 9 April 2009, in final form 18 June 2009
Published 22 July 2009
Online at stacks.iop.org/PMB/54/4835

Abstract

Although the calculation of the surface average of the low-frequency current density distribution over a cross-section of 1 cm^2 is required by ICNIRP guidelines, no reference averaging algorithm is indicated, neither in the ICNIRP guidelines nor in the Directive 2004/40/EC that is based on them. The lack of a general standard algorithm that fulfils the ICNIRP guidelines' requirements is particularly critical in the prospective of the 2004/40/EC Directive endorsement, since the compliance to normative limits refers to well-defined procedures. In this paper, two case studies are considered, in which the calculation of the surface average is performed using a simplified approach widely used in the literature and an original averaging procedure. This analysis, aimed at quantifying the expected differences and to single out their sources, shows that the choice of the averaging algorithm represents an important source of uncertainty in the application of the guideline requirements.

(Some figures in this article are in colour only in the electronic version)

Introduction

The perspective of the enactment of the 2004/40 EU Directive (EU 2004) has led to a detailed analysis of the technical applicability of its requirements. Particular attention has been paid to the calculation of the surface average of the low-frequency current density introduced by the ICNIRP guidelines (ICNIRP 1998) and adopted by the Directive itself.

According to these guidelines, in order to assess compliance with exposure limit values, current densities have to be averaged over a cross-section of 1 cm^2 at every point of the

exposed body. This requirement is also prescribed by Note 3 of table 1 of the Directive, which states that 'because of the electrical inhomogeneity of the body, current densities should be calculated as averages over a cross-section of 1 cm^2 perpendicular to the current direction'.

Also important, the 'target tissues' for this averaging are the tissues of the central nervous system (CNS). In fact, Note 2 of the same table specifies that 'the exposure limit values on the current density are intended to protect against acute exposure effects on central nervous system tissues in the head and trunk of the body'.

The availability of high-resolution numerical body models, reliable computational methods and high-performance digital computers makes today numerical techniques the preferred choice to calculate the current density distribution inside a human body. In spite of this, the EU Directive and the ICNIRP guidelines neither define a reference surface averaging procedure nor indicate how to proceed when the 1 cm^2 averaging surface intersects tissues not belonging to the CNS.

This latter problem is discussed in recent papers (Bahr *et al* 2007, Dimbylow 2008), where simplified averaging algorithms are applied. The use of a simplified algorithm does not affect the validity of the analysis carried out in these papers, since they are focused on the CNS/non-CNS limitation issue. Nevertheless, we were not able to find any *rigorous* averaging algorithm in the literature, neither in recent nor in older papers.

In this paper, a procedure that aims to rigorously implement the geometrical definition of the surface average of a vector field is developed and applied to a couple of case studies, both characterized by linear polarization: (1) a double-layer cylinder exposed to a homogeneous magnetic field parallel to the cylinder axis and (2) a human model exposed to the non-homogeneous magnetic field generated by an induction heater. In both cases, the results are compared to those given by the simplified algorithm introduced in Dawson *et al* (2002). The discussion of the examples is focused on the averaging procedure and does not deepen the limitation of the average to CNS tissue, which is widely presented in the previously cited papers.

Dawson's averaging algorithm

Dawson *et al* (2002) introduced a simplified algorithm for current density averaging. According to it the components of the current density average 'associated with a given voxel are computed by averaging the perpendicular components of current density over squares with 1 cm edges centred on the voxel and parallel to the three principal Cartesian planes. The resulting vector field is treated similarly to the current density itself in dosimetry computations'.

This algorithm introduces two main approximations.

- First, it uses square cross-sections that intersect different portions of surrounding voxels, depending on their orientations (figures 1(a) and (b)). Actually, the squares are aligned with voxel faces (figure 1(a)) to simplify the calculation procedure; although this is a convenient orientation, it is in general an arbitrary choice.
- Second and more important, the cross-sections used to average the current density are not necessarily perpendicular to the direction of the current (indicated with $\vec{V}$), as required by the Directive. In particular, three separate 1 cm^2 squares are considered, each perpendicular to one of the three directions defined by the edges of the voxels. In figure 2, an example in two dimensions is shown.

In the following, we will refer to this algorithm as the 'simplified averaging algorithm' or just the 'simplified algorithm'.

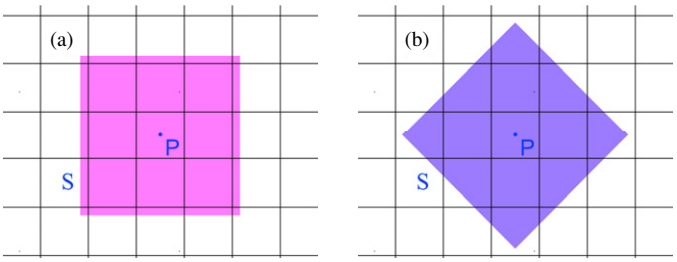

Figure 1. Orientation of the averaging squares used in the simplified algorithm. (a) The usual orientation; (b) a possible different choice. The grid represents the voxels' faces on a generic averaging plane parallel to a voxel face (3 mm voxel resolution is supposed). P is the application point of the surface average. S is the 1 cm^2 averaging square. Different voxels contribute to the surface average, depending on the chosen orientation, as clearly shown.

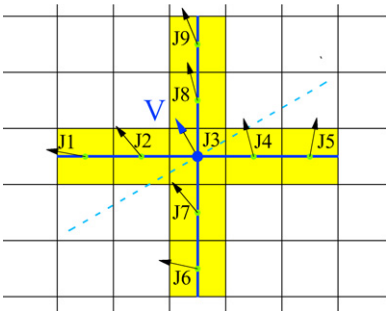

Figure 2. Averaging planes in the Dawson's simplified algorithm. The vector V indicates the direction of the current density at the application point. The pixels that contribute to the surface average are highlighted. The direction of the current density in every evidenced pixel is represented with an arrow and a J_i label. The cross-section perpendicular to V is indicated by a dashed line. Voxels J1 to J5 contribute to the vertical component of the average and J6 to J9 to the horizontal component. The overall average in the direction of the current density is then the magnitude of the vector formed from these two components.

Rigorous averaging procedure

The simplified algorithm obviously produces exact results when applied to uniform vector fields, but gives rise to errors in less trivial situations. For this reason, we developed a procedure that aims to implement the rigorous definition of the cross-section averaging of a linearly polarized vector field. This procedure—which will be called 'rigorous averaging procedure' downward—consists in the following steps, which should be applied to each voxel where the average has to be calculated (the so-called application point of the averaging process).

- A plane ('averaging plane') is chosen that is perpendicular to the current density at the application point.
- A circular 1 cm^2 cross-section, lying on the averaging plane and having centre at the application point, is considered. The choice of a circular profile avoids orientation ambiguity on the surface plane as in the case of square profiles (figure 1).
- The intersecting section S_i of every voxel with the circular cross-section of the previous step is determined. Since the averaging plane is not, in general, perpendicular to a voxel

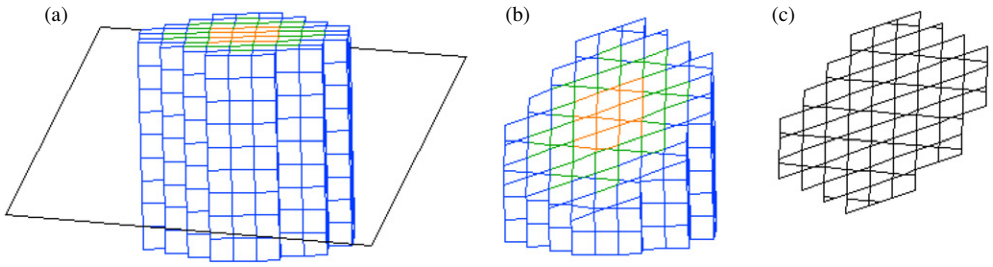

Figure 3. (a) Cylindrical structure built with cubic voxels. (b) Cylindrical structure cut by a plane not perpendicular to the axis of the cylinder. (c) Plane sections of the cut voxels.

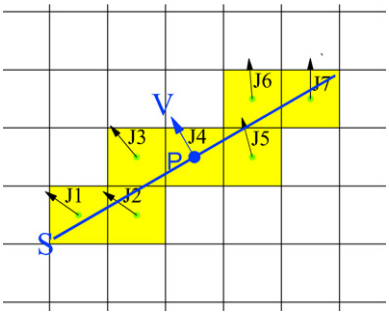

Figure 4. Averaging planes in the rigorous procedure. The vector V indicates the direction of the current density at the application point. The pixels that contribute to the surface average are highlighted. The direction of the current density in every evidenced pixel is represented with an arrow and a J_i label. The averaging cross-section is now actually perpendicular to the direction of the current in the central voxel.

face, this intersecting section can assume the form of a generic polygon with 3, 4, 5 or 6 sides, as reported in Reveilles (2001). This can be noted in figure 3, where a cylindrical structure built with cubic voxels is cut by a plane not perpendicular to the axis of the cylinder.

- The cross-section average of current density is calculated in every voxel according to (1). The current density is assumed to be uniform inside each voxel and therefore on each voxel plane section:

$$J_{\text{avg}} = \frac{\sum_{i=1}^{N} [S_i(\vec{J}_i \cdot \vec{V})]}{\sum_{i=1}^{N} S_i}. \tag{1}$$

The same 2D example of figure 2 is presented in figure 4, now with reference to the rigorous averaging procedure. It can be noted that voxels that contribute to the surface average are not the same as in figure 2.

The steps that compose the rigorous procedure can be performed using the standard techniques of computational geometry. Some details about non-trivial ones are furnished in the following.

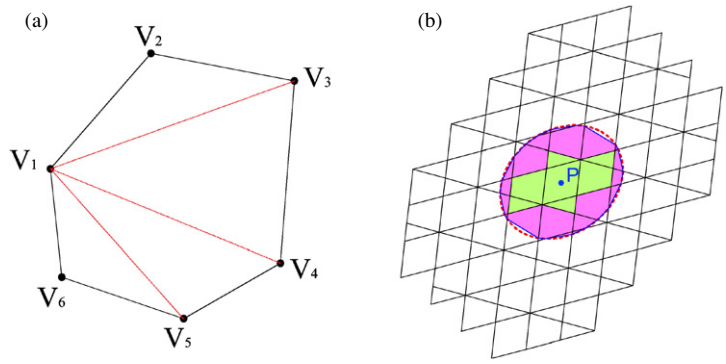

Figure 5. Implementation details. (a) Breakdown of a convex polygon into triangles; the vertex V_1 is chosen as pivot for the process. (b) Correction of the circular surface border. The application point P is the intersection point of the cylinder axis and the averaging plane. The sections totally contained or partially contained in the averaging circle (dashed line) are marked differently. All the circle arcs delimited by the intersection points with the section edges are represented with their chords. The effective averaging area (highlighted area) is less than 1 cm^2 (dashed circle area).

Pre-selection of voxels close to the application point

The averaging procedure must in general be applied to every phantom voxel constituted by one of the CNS tissues. Since this algorithm often requires processing of voxels close to the averaging application point, it is convenient to pre-select all the voxels contained in the smallest parallelepiped able to embrace the circular averaging surface. The faces of the parallelepiped are parallel to those of the voxel, while the length of its longer edge depends on the radius of the averaging circle (actually 0.564 cm) and on the orientation of the averaging plane.

Selection of voxels intersecting the averaging surface

The voxels that actually intersect the averaging plane are selected among the pre-selected ones described in the previous paragraph. The number of pre-selected voxels obviously depends on the voxel size. Even with a resolution as high as 1 mm, a 'brute force' approach is feasible with moderate averaging time. For each pre-selected voxel, 12 tests should be performed in order to assess if its edges intersect the averaging surface.

Area of the section of a voxel intersected by a generic plane

The area of the section of a voxel intersected by a plane is computed through the following steps:

- the intersection points of the edges of the voxel with the averaging plane are determined;
- these intersection points are ordered along the perimeter of the section;
- the area of the section is computed choosing an intersecting point as pivot and breaking down the section itself into triangles, as illustrated in figure 5(a). This approach is valid since the voxel sections are convex polygons.

Circular surface border correction

If the plane section of a voxel is not entirely contained in the circular averaging surface, only the internal part of the section should be considered in (1). The effective plane section averaging area is set replacing the circle arc (delimited by the intersection points with the section edges) with its chord (figure 5(b)). A more precise representation of the circle can easily be obtained

by adding points along every considered arc. This is more and more necessary with increasing voxel size.

Limitation to the central nervous system

When the application point of the averaging cross-section is close to a surface separating an organ of the CNS from a different tissue, the averaging cross-section will possibly intersect voxels that do not belong to the CNS. For instance, the spinal cord has in many cases a cross-section smaller than 1 cm^2 (Dimbylow 2008). Another critical case is the retina with its thin curved shape. Current density is not necessarily perpendicular to the retina so the averaging surface can 'cut' the retina itself. Furthermore, the averaging surface has to be a plane figure (ICNIRP guidelines require averaging over a 'cross-section') and would not encompass the retina (due to its curved shape) even if the current density were perpendicular to the retina itself.

In these situations, it should be decided if the contributions to the average coming from tissues not belonging to the CNS have to be considered.

Different approaches have been presented in the literature, in the past (Dawson *et al* 2002) and more recent works (Bahr *et al* 2007, Crozier *et al* 2007, Dimbylow 2008). In the following examples we adopted the 'full averaging' approach (Dawson *et al* 2002), according to which the averaging application point is always taken in a voxel that belongs to the central nervous system, but the contributions of all other voxels (even not belonging to the CNS) that intersect the averaging plane are also fully considered. This choice is inspired by Note 2 to table 4 of the ICNIRP guidelines (ICNIRP 1998), which introduce the current density averaging 'because of the electrical inhomogeneity of the body'. If the aim of the averaging is to take into account the electrical inhomogeneity, it seems a nonsense to exclude some voxels once the averaging cross-section has been defined.

Both simplified and rigorous algorithms can be applied with other approaches such as zero weighting the contributions of non-CNS tissues or restricting the surface average to less extended surfaces that intersect only CNS tissues if necessary. A detailed analysis in that sense is out of the scope of this work since limitation to CNS tissues is a distinct issue from surface averaging on which the paper is focused and also because this subject has already been studied in the previously cited papers. On the other hand, a hint on what happens using different averaging strategies can be useful to give a wider perspective on the problem. This point is addressed in the paragraph before the conclusions, with reference to the second example.

Examples

In the following paragraphs two examples are discussed. The first one refers to a double-layer cylinder exposed to a homogeneous axial magnetic field. The second example is a more realistic case of a digital body model exposed to the non-uniform magnetic field generated by a solenoid.

Double-layer cylinder exposed to a homogeneous axial magnetic field

The double-layer cylinder of figure 6(a) is considered, exposed to a 1 T homogeneous magnetic flux density field, directed parallel to the cylinder axis and having a frequency of 1 Hz. The inner layer has a radius of 2 cm and a conductivity of 1 S m^{-1}, while the radius of the cylinder is 4.5 cm and the conductivity of the outer layer is 4 S m^{-1}. The cylinder is segmented in cubic voxels having 1 mm long edges.

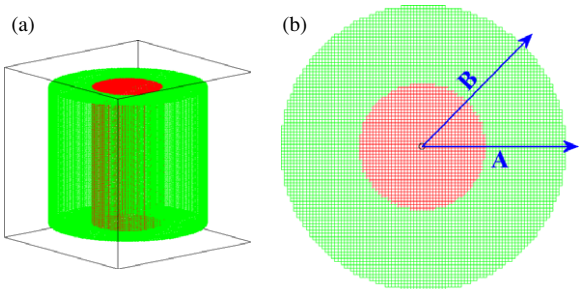

Figure 6. First example. (a) The exposed cylinder; (b) the two reference directions A and B.

Table 1. Averaged current density, the simplified algorithm ($J_{\text{avg-simp}}$).

Layer	Max (mA m^{-2})	Mean (mA m^{-2})
Inner	160.39	59.38
Outer	524.94	382.14

Two directions A and B are chosen (figure 6(b)) to compare the results of the two averaging procedures.

In this case, the local peak current density distribution is analytically known. At every point of the cylinder, the current density lies in the plane perpendicular to the cylinder axis and is tangent to the circle centred in the same axis. The two averaging algorithms are applied to the analytically calculated current density distribution. Due to the axial symmetry of this distribution, the surface average of the current density calculated along the two directions A and B should be exactly the same in the ideal case. Since the problem is represented with the cubic voxels of finite size, some differences are expected, due to the well-known 'stair-casing effect' (Dawson *et al* 2001). These differences will concentrate in proximity of the interfaces, being caused by the discrete representation of a curved surface.

In figure 7(a), the averaged current density distribution, calculated with the simplified algorithm along the two considered directions A and B, is shown; the local peak of the current density is also presented. In figure 7(b), the same results are reported, as given by the rigorous procedure.

By comparing the two figures, it can be noted that the results of the simplified algorithm depend more on the chosen direction. This is due to the inaccurate choice of the orientation of the averaging surface.

In figures 7(c) and (d) the same results of the two previous figures are rearranged, taking directions A and B separately into account.

It can be noted that the differences are higher along direction B (figure 7(d)), where the current density is not parallel to the edges of the voxel; once again, these differences can be attributed to the unsuitable choice of the averaging surface in the simplified algorithm. In contrast, the minor differences that can be noted along direction A (figure 7(c)) should be attributed to the different averaging shapes adopted by the two algorithms (a square and a circle).

The analysis of the results continues in tables 1 and 2, where $J_{\text{avg-simpl}}$ and $J_{\text{avg-rigorous}}$ are the surface-averaged current densities calculated, respectively, using the simplified and the rigorous averaging procedure.

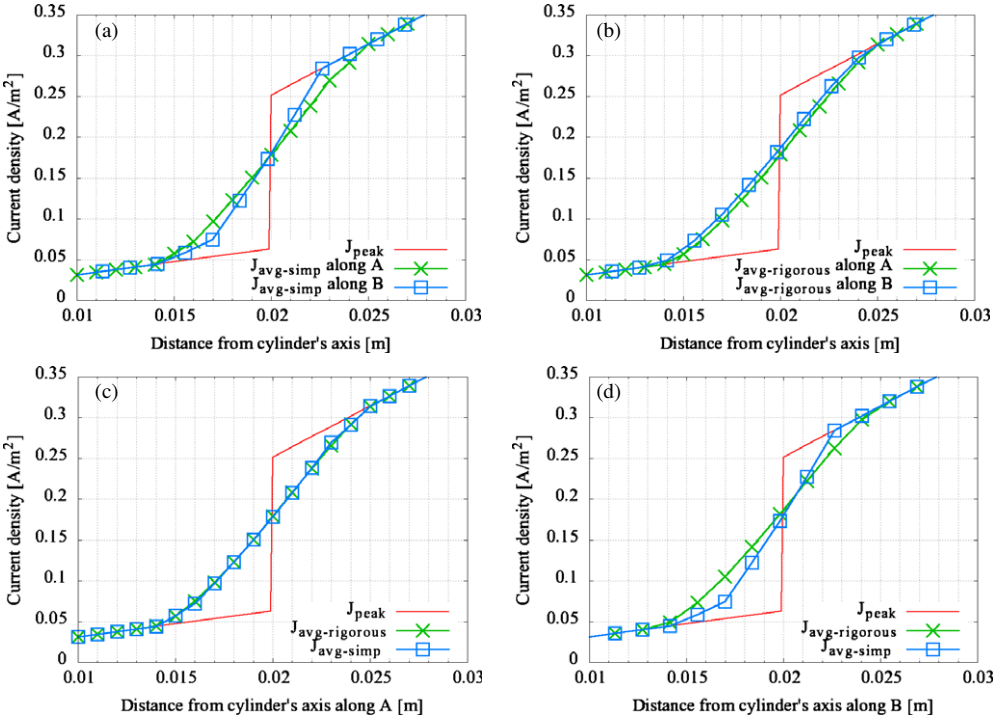

Figure 7. (a) Current density surface average calculated along directions A and B with the *simplified* algorithm; (b) current density surface average calculated along directions A and B with the *rigorous* procedure; (c) current density surface average calculated along direction A with both the *simplified* and the *rigorous* algorithms; (d) current density surface average calculated along direction B with both the *simplified* and the *rigorous* algorithms.

Table 2. Averaged current density, rigorous procedure ($J_{\text{avg-rigorous}}$).

Layer	Max (mA m^{-2})	Mean (mA m^{-2})
Inner	161.22	62.46
Outer	510.29	374.98

In tables 3 and 4, the deviations between the two algorithms are further exploited. In order to draw table 3, the local relative difference LRD between $J_{\text{avg-simp}}$ and $J_{\text{avg-rigorous}}$ was calculated with equation (2) for each cell of the cylinder:

$$\text{LRD} = \left| \frac{J_{\text{avg-rigorous}} - J_{\text{avg-simp}}}{J_{\text{avg-rigorous}}} \right|. \tag{2}$$

Then, the maximum and the mean values of all these differences were determined and reported in the tables. As can be noted, the maximum LRD value reaches 33.4%.

In table 4, the relative difference OMRD between the overall maximum values of the averaged current densities $J_{\text{avg-simp}}$ and $J_{\text{avg-rigorous}}$, calculated with equation (3), is reported:

$$\text{OMRD} = \left| \frac{\max(J_{\text{avg-rigorous}}) - \max(J_{\text{avg-simp}})}{\max(J_{\text{avg-rigorous}})} \right|. \tag{3}$$

Table 3. Maximum and mean relative differences between the simplified and the rigorous algorithms in the cylinder cells.

Layer	Max (LRD)	Mean (LRD)
Inner	33.4%	3.7%
Outer	29.3%	2.2%

Table 4. Relative difference between the overall maximum values of the averaged current densities calculated with the simplified and the rigorous algorithms.

Layer	OMRD
Inner	0.5%
Outer	2.9%

As can be seen, this maximum value (which is the one to be considered in order to assess compliance with EU limits) is far less prone to differences between the algorithms than the local values.

Digital body model exposed to the magnetic field generated by a solenoid

The case described in Zoppetti and Andreuccetti (2008) is considered as a second example for the comparison of the surface averaging algorithms.

The source is a small induction furnace used in the gold industry, modelled here with a solenoid. The body model used to represent the exposed subject was prepared by processing the Visible Human Project Dataset and is segmented into 3 mm cubic cells. This example concerns the exposure of a worker standing in front of the furnace with extended arms, as if he were putting gold into it (figure 8). In this context, the two averaging algorithms are applied to the calculated distribution of the induced current density.

The analysis will focus on CNS and some other significant tissues. In the digital body model used in this work, the spinal cord and the nerves are not distinguishable, but this is not a major limitation, as our attention is focused on differences between the results of different averaging algorithms rather than on compliance assessment.

In table 5, the maximum, the mean and the 99th percentile of the values of the induced current density distribution in the body model cells are reported. The 99th percentile is considered since it can be assumed to represent the maximum value purified from artefacts like digitalization errors (Hirata *et al* 2001).

The two averaging algorithms are applied to this distribution, leading to the results reported in table 6 (simplified algorithm) and table 7 (rigorous procedure).

In table 8, the maximum, the mean and the 99th percentile values of the LRD between $J_{\text{avg-simp}}$ and $J_{\text{avg-rigorous}}$, calculated with equation (2) for each cell of the body model, are reported. As can be noted, cell-to-cell maximum ratios can be up to 25 dB (i.e. ratios above 300 in the linear scale). In terms of 99th percentile, local ratios are lower but can exceed 6 dB (i.e. ratios above 4 in the linear scale).

Overall differences OMRD and O99RD (calculated by means of equations (3) and (4), respectively) reported in table 9 are highly relevant, since they represent differences in terms of the values that should be compared with the EU limits in order to assess compliance. As can

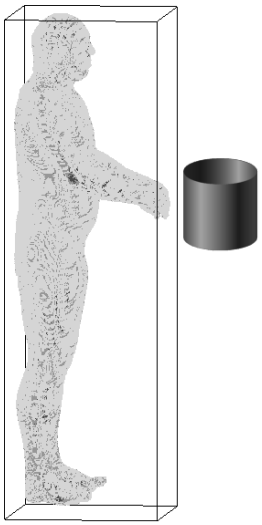

Figure 8. The exposure scenario of the second example.

Table 5. Maximum, mean and 99th-percentile values of the induced current density distribution in the body model cells.

Tissue	Max (mA m^{-2})	Mean (mA m^{-2})	99% (mA m^{-2})
Brain grey matter	7.59	1.88	4.68
Brain white matter	4.19	1.34	2.88
Cerebellum	11.01	2.48	6.87
Cerebro spinal fluid	112.79	19.97	64.70
Nerve/spinal cord	19.29	1.85	10.03
Fat	91.82	2.20	7.73
Muscle	235.13	15.98	59.34

Table 6. Averaged current density, the simplified algorithm ($J_{\text{avg-simp}}$).

Tissue	Max (mA m^{-2})	Mean (mA m^{-2})	99% (mA m^{-2})
Brain grey matter	7.71	2.16	5.04
Brain white matter	4.97	1.50	3.27
Cerebellum	9.59	2.66	7.79
Cerebro spinal fluid	77.89	15.63	48.02
Nerve/spinal cord	19.10	3.27	11.84
Fat	61.73	3.09	13.31
Muscle	164.57	15.24	54.00

be seen, in this case differences are relevant considering both maximum and 99th-percentile values:

$$\text{O99RD} = \left| \frac{99\%(J_{\text{avg-rigorous}}) - 99\%(J_{\text{avg-simp}})}{99\%(J_{\text{avg-rigorous}})} \right|. \tag{4}$$

Table 7. Averaged current density, rigorous procedure ($J_{\text{avg-rigorous}}$).

Tissue	Max (mA m^{-2})	Mean (mA m^{-2})	99% (mA m^{-2})
Brain grey matter	12.51	2.60	7.50
Brain white matter	8.98	1.71	4.54
Cerebellum	16.11	2.90	11.10
Cerebro spinal fluid	32.84	8.03	25.95
Nerve/spinal cord	38.15	5.55	19.82
Fat	87.72	4.49	27.12
Muscle	85.30	14.00	47.39

Table 8. Maximum, mean and 99th–percentile values of the relative differences between the simplified and rigorous algorithms in the body cells.

Tissue	Max (LRD)	Mean (LRD)	99% (LRD)
Brain grey matter	104.9%	20.6%	61.6%
Brain white matter	78.8%	11.6%	57.7%
Cerebellum	72.2%	9.0%	54.4%
Cerebro spinal fluid	490.7%	120.6%	328.1%
Nerve/spinal cord	97.1%	38.2%	71.6%
Fat	36378.7%	24.9%	67.7%
Muscle	17716.4%	10.9%	86.6%

Table 9. Relative difference between the overall maximum values of the averaged current densities calculated with the simplified and the rigorous algorithms.

Tissue	OMRD	O99RD
Brain grey matter	38.4%	32.8%
Brain white matter	44.7%	28.0%
Cerebellum	40.5%	29.8%
Cerebro spinal fluid	137.2%	85.0%
Nerve/spinal cord	49.9%	40.3%
Fat	29.6%	50.9%
Muscle	92.9%	13.9%

Effects of the averaging strategy

In the following tables the full averaging (F) strategy, used in the previous paragraphs, is compared with a tissue-specific approach (T), limited to CNS tissue (not considering cerebro spinal fluid as part of CNS).

According to Dawson *et al* (2002), the T average is computed in a similar manner to F, except that, in the averaging, current density contributions associated with a dissimilar tissue from that of the target set, are zero-weighted.

In table 10 overall differences OMRD and O99RD between the two averaging algorithms are reported in the case of a T approach.

The comparison of tables 9 and 10 shows that differences between averaging algorithms are smoothed by the choice of a T averaging strategy.

Table 10. Relative difference between the overall maximum values of the averaged current densities calculated with the simplified and the rigorous algorithms. Tissue-specific average, restricted to the set of tissues reported in rows.

Tissue	OMRD	O99RD
Brain grey matter	15.6%	23.6%
Brain white matter	13.2%	6.2%
Cerebellum	25.7%	10.1%
Nerve/spinal cord	19.0%	46.2%

Table 11. Relative difference between the overall maximum values of the averaged current densities calculated with the simplified algorithm using a full average (F) and a tissue-specific (T) averaging strategy.

Tissue	$\mathrm{OMRD}_{\mathrm{F-T}}$	$\mathrm{O99RD}_{\mathrm{F-T}}$
Brain grey matter	22.2%	21.2%
Brain white matter	20.4%	12.7%
Cerebellum	10.6%	23.3%
Nerve/spinal cord	23.9%	30.9%

Table 12. Relative difference between the overall maximum values of the averaged current densities calculated with the rigorous algorithm using a full average (F) and a tissue-specific (T) averaging strategy.

Tissue	$\mathrm{OMRD}_{\mathrm{F-T}}$	$\mathrm{O99RD}_{\mathrm{F-T}}$
Brain grey matter	58.5%	57.2%
Brain white matter	49.3%	32.9%
Cerebellum	57.7%	51.1%
Nerve/spinal cord	68.0%	71.5%

This is coherent with what is reported in figure 7(d) that shows how differences between the algorithms are mainly due to the different orientations of the averaging surfaces close to interfaces, which can provoke the inclusion in the average of different portions of high-conductivity districts. The T approach avoids the inclusion of cerebro spinal fluid and excludes the main cause of the difference between the two averaging algorithms.

In tables 11 and 12, overall differences between the F and T approaches (calculated by means of equation (5)) are reported respectively for the simplified and rigorous algorithms:

$$\begin{aligned} \mathrm{OMRD}_{\mathrm{F-T}} &= \left| \frac{\max(J_{\mathrm{avg-F}}) - \max(J_{\mathrm{avg-T}})}{\max(J_{\mathrm{avg-F}})} \right| \\ \mathrm{O99RD}_{\mathrm{F-T}} &= \left| \frac{99\%(J_{\mathrm{avg-F}}) - 99\%(J_{\mathrm{avg-T}})}{99\%(J_{\mathrm{avg-F}})} \right|. \end{aligned} \tag{5}$$

Comparison between tables 11 and 12, once again, highlights how differences between F and T are emphasized by the choice of the 'rigorous' algorithm. This is coherent with what has been observed comparing tables 9 and 10.

Conclusions

A problem encountered when assessing compliance with ICNIRP guidelines has been discussed. While the calculation of the cell-by-cell local induced current density distribution can today be considered a rather straightforward process, difficulties arise when trying to calculate its spatial average, since this key question is not completely specified, neither in the 2004/40 EU directive, nor in the ICNIRP guidelines and the scientific literature.

Two different averaging methods were considered: a simplified algorithm and a more rigorous procedure. While the former is widely used in the literature, but does not implement the precise requirements of the directive, the latter considers an averaging cross-section perpendicular to the current density, as required by the ICNIRP guidelines. The two methods are tested with reference to two different case studies: a double-layer cylinder exposed to a homogeneous field and a human model exposed to an induction heater.

The discussion of the first case study allows us to separate the sources of differences between the two algorithms. Such differences (small in the specific case) are linked to two distinct aspects: different shapes and different orientations of the averaging surfaces.

In contrast, considerable differences were evidenced when applying the two algorithms to a more realistic case, with a non-homogeneous field distribution and an anatomical digital body model. This can be considered as an important source of methodological uncertainty that could be avoided if a reference algorithm were indicated in the normative framework.

A revisiting of the normative is desirable, particularly if one considers that the concept of the plane perpendicular to the current density is not even applicable in the case of elliptical or circular polarization, since current density direction changes with time.

In the meanwhile, it should also be noted that, even if the simplified algorithm does not rigorously implement the normative requirements, it is applicable also to the case of circular or elliptical polarization.

Acknowledgment

The research activity which the work described in this paper was based upon, was partially carried out in the framework of the contract no 18455 between IFAC-CNR and Trenitalia Spa, signed on 20 December 2007.

References

Bahr A, Bolz T and Hennes C 2007 Numerical dosimetry ELF: accuracy of the method, variability of models and parameters, and the implication for quantifying guidelines *Health Phys.* **92** 521–30

Crozier S, Wang H, Trakic A and Liu F 2007 Exposure of workers to pulsed gradients in MRI *J. Magn. Reson. Imaging* **26** 1236–54

Dawson T W, Caputa K and Stuchly M 2002 Magnetic field exposures for UK live-line workers *Phys. Med. Biol.* **47** 995–1012

Dawson T W, Potter M and Stuchly M 2001 Evaluation of modelling accuracy of power frequency field interactions with the human body *ACES J.* **16** 162–72

Dimbylow P 2008 Quandaries in the application of the ICNIRP low frequency basic restriction on current density *Phys. Med. Biol.* **53** 133–45

EU 2004 Directive 2004/40/EC of the European Parliament and of the Council of 29 April 2004 on the minimum health and safety requirements regarding the exposure of workers to the risks arising from physical agents (electromagnetic fields) *Off. J. Eur. Union Legis. 184* **47** 1–9

Hirata A, Caputa K, Dawson T W and Stuchly M 2001 Dosimetry in models of child and adult for low-frequency electric field *IEEE Trans. Biomed. Eng.* **48** 1007–12

ICNIRP 1998 Guidelines for limiting exposure to time-varying electric, magnetic, and electromagnetic fields (up to 300 GHz) *Health Phys.* **74** 494–522

Reveilles J P 2001 The geometry of the intersection of voxel spaces *Electron. Notes Theor. Comput. Sci.* **46** available at http://liris.cnrs.fr/isabelle.sivignon/Articles/Cours/reveilles_intersection_voxels2001.pdf

Zoppetti N and Andreuccetti D 2008 Compliance with EU basic restrictions near induction furnaces used in precious metal industry: a 3d numerical dosimetric analysis using the scalar potential finite difference (SPFD) technique and a posturable digital body model *Proc. 5th Int. Workshop on Biological Effects of EMFs (Palermo, IT, 28 September–2 October 2008)*